Changes in the Microstructure and Characteristics of Carbon/Carbon Composites with Mesophase Mesocarbon Microbeads Added During Graphitization

Hsien-Lin Hu,[1] Tse-Hao Ko,[1] Wen-Shyong Kuo[2]

[1]*Department of Materials Science and Engineering, Feng Chia University, Taichung, Taiwan, Republic of China*
[2]*Department of Aeronautical Engineering, Feng Chia University, Taichung, Taiwan, Republic of China*

Received 15 September 2004; accepted 3 March 2005
DOI 10.1002/app.22394
Published online in Wiley InterScience (www.interscience.wiley.com).

ABSTRACT: Carbon/carbon (C/C) composites were prepared from oxidative PAN fiber felts, a resol-type phenolic resin, and mesophase pitch derived from coal tar. In this study, the effects on mesocarbon microbeads (MCMBs), flexural strength, flexural moduli, electric conductivity, and thermal conductivity of C/C composites with a mesophase content ranging from 0 to 30 wt % were examined during pyrolysis. The results show that the C/C composite with the addition of 10–30 wt % mesophase had a higher density, greater stacking size, and higher preferred orientation than the C/C composites without any mesophase during heat treatment. These composites also exhibited an improvement in flexural strength from 19.7 to 30.3%. The flexural moduli of these composites with mesophase added increased by 15.1 to 31.3% compared to that with no mesophase added. These composites also showed improved electric conductivity, from 15.1 to 43.7%, and thermal conductivity, from 12 to 31.3%. © 2005 Wiley Periodicals, Inc. J Appl Polym Sci 98: 2178–2190, 2005

Key words: composites; fibers; microstructure; pyrolysis; Raman spectroscopy

INTRODUCTION

Carbon fiber/carbon matrix composites are regarded as materials with the best structures for potential application in high-temperature environments because of their light weight, high thermal shock resistance, low thermal expansion, and relatively high strength/stiffness at high temperatures.[1–3] With their combined excellent thermal shock, ablation resistance, and unique mechanical properties at high temperatures, carbon/carbon (C/C) composites can be used in industry for the manufacture of items such as brakes and nozzles. They can also be used at intermediate temperatures (200–1000°C) in applications in which reinforced polymers cannot be used, such as connecting rods and pistons. In earlier research, expensive, high-modulus carbon fibers and techniques have been used to produce these composites. However, a high demand for industrial applications has resulted in the development of alternative fabrication routes with lower costs and controlled mechanical and thermal properties. In aerospace applications, two dimension–C/C composites have been made from woven carbon fabrics as reinforcements.

The correct types of matrix and fiber must be used to make C/C composites; the physical and chemical traits of the composites depend strongly on the precursors of the matrix used and the method of fabrication. The nature of the bonding between the fiber and matrix deeply affects the performance and mechanical properties of the C/C composites.[4,5] Phenolic, polyfufuryalcohol resin and pitch normally serve as precursors of the matrix. Chemical vapor infiltration is considered the optimal approach to fabricating a matrix with ideal physical and chemical properties,[6,7] yet this method for depositing carbon as a matrix is too long and too costly. Liquid infiltration of mesophase pitch is seen as another means of generating ideal physical and chemical characteristics for C/C composites. Therefore, several have studied this issue and elucidated limits of the use of mesophase pitch as a matrix precursor.[8,9] Unfortunately, mesophase pitch MCMBs as a matrix precursor for C/C composites cannot infiltrate reinforcements effectively enough. We used a resol-type phenolic resin, mixed with mesophase pitch, to form matrix precursors in a previous work.[10] Accordingly, the resol-type phenolic resin could easily infiltrate the reinforcement and bind the mesophase MCMB sphere. In our previous study, we found that mesophase additives successfully improved thermal conductivity MCMB and reduced weight loss and linear shrinkage. Still, composites were only heat-treated up to 1000°C for that task. This study extended the first to elucidate connections between the microstruc-

Correspondence to: H.-L. Hu (watterhu@pchome.com.tw).
Contract grant sponsor: National Science Council of the Republic of China; contract grant number: NSC 92-2216-E035-001.

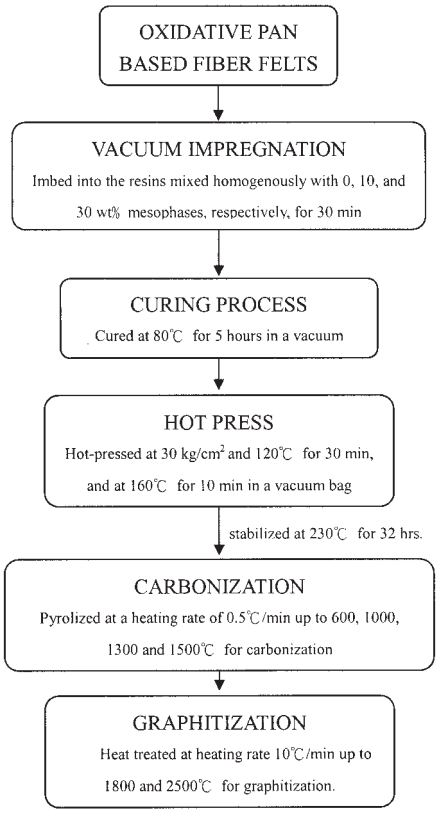

Figure 1 Flow diagram of the C/C composite fabrication procedure.

ture and physical properties of the composites during graphitization. Effects on the microstructure of adding mesophase pitch MCMBs to the composites and the interaction between the fiber and matrix during graphitization are discussed.

EXPERIMENTAL

Raw materials

The C/C composites were reinforced with oxidative polyacrylonitrile (PAN) fiber felts (Toho Rayon Co., Ltd., Japan). A resol-type phenol–formaldehyde resin (Chang Chum Petrochemical Industry Co., Taiwan, Tokyo) was used as a matrix precursor; mesophase spheres MCMBs (China Steel Chemical Co., Taiwan, Tokyo) were extracted from coal tar. The characteristics of the mesophase pitch MCMB and the oxidative PAN fiber felts were specified in our previous article.[10]

Fabrication

The resol-type phenol–formaldehyde resin was dissolved in methanol. Then, 10 and 30 wt % mesophase spheres MCMBs were added to and mixed with the phenolic resin. Figure 1 presents the fabrication procedures. First, oxidative PAN-based fiber felts were embedded into the resin mixed homogeneously with 0, 10, and 30 wt % mesophase spheres MCMB for 30 min *in vacuo*. Second, impregnated samples were cured at 80°C for 2 h and hot-pressed at 30 kg/cm^2 and 120°C for 30 min and at 160°C for 10 min Then, the polymer composites were cut to the appropriate sizes. Finally, the cut samples were stabilized at 230°C and pyrolyzed at a heating rate of 0.5°C/min up to 600, 1000, 1300, and 1500°C for carbonization; these composites were heat-treated at a rate of 10°C/min up to 1800 and 2500°C for graphitization.

Measurements

A Rigaku X-ray diffractometer with a Cu Kα radiation source was used to determine d spacing and stacking size (L_C; i.e., the stacking height of the layer planes) of the composites; a Scherrer equation[11] was used to calculate L_C from the width of a (002) reflection (B):

$$L_c = \frac{k\lambda}{B \cos \theta} \tag{1}$$

where $\lambda = 0.154$ nm, k is the apparatus constant ($k = 1.0$), and B is half the width of the C/C composites. The width increased as L_C declined. The Raman spectrum (Renishaw Raman imaging microscopy system) was used to ascertain the microcrystalline planar size (L_a) and I_D/I_G ratio (R) as follows:[12]

$$R = \frac{I_D}{I_G} \tag{2}$$

$$L_a = 44\left(\frac{I_D}{I_G}\right)^{-1} \tag{3}$$

where I_D is intensity of the peak at 1350 cm^{-1} caused by sp^2 bonding in carbon and I_G is intensity of the peak at 1890 cm^{-1} caused by sp^3 bonding in carbon.

The flexural strength of the composites was determined by the three-point bending method according to ASTM D 790. Fractured composites were examined with a scanning electron microscope (Hitachi S3000N). Weight loss was calculated as follows:

$$W_2(\%) = \left(\frac{W_O - W_1}{W_O} \times 100\%\right) \tag{4}$$

where W_O is the original weight before heat treatment, W_1 is the weight after heat treatment, and W_2 is weight loss of the composites. The C/C composites were studied with an Olympus BHT apparatus on polished surfaces. The texture of the aromatic layers with respect to the fiber and mesophase was determined crossed polarizer with a λ retarder plate.

Real density was measured by AccuPyc 1330 Pycnometer in helium. The thermal conductivity of C/C composites was measured with a Micro300 (Holome-

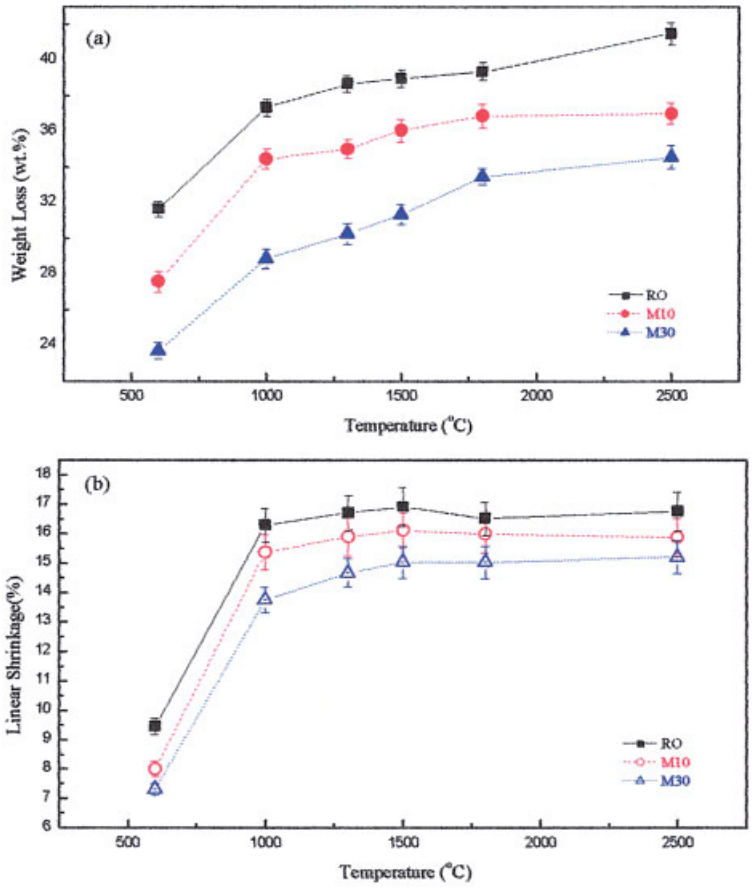

Figure 2 Physical changes in the composites at different HTTs: (a) weight loss and (b) shrinkage.

trix) according to ASTM 1461 C 714. The electrical resistance and conductivity of composites were gauged by Mitsubishi Chemical MCP-T600 and the four-point probes method. The open porosity of the C/C composites was measured according to ASTM D 570.

RESULTS AND DISCUSSION

Physical changes during carbonization and graphitization

The R0, M10, and M30 composites were pure resin, the composite derived from resin mixing with 10 wt % mesophase, and the composite derived from resin mixing with 30 wt % mesophase MCMBs, respectively. Some small molecules volatized from the fiber and the matrix during carbonization, noncarbon elements removed as volatiles, such as H_2O, HCN, NH_3, N_2, CO_2, CO, and other gases.[13–15] The reaction of the oxidative PAN fiber proceeded below 450°C because a crossing reaction occurred between two ladder polymers. Above 450°C, the carbon basal plane from the ladder polymer was lengthened and broadened. In resins, aromatic ribbon molecules condense, volatilizing species of low molecular weight.[16] Such reactions induced weight loss in the C/C composites during heat treatment, as shown in Figure 2(a). The weight loss of the composites with mesophase spheres MCMBs added was less than that of the composites without mesophase spheres MCMBs. The mesophase was a mild product of pitch carbonization; it formed as the temperature rose from 400 to 600°C.[17,18] Numerous small molecules became resealed during the fabrication of the mesophase spheres. The weight loss of the mesophase spheres after carbonization was less than for the phenolic resin, a factor thought to reduce the weight loss of the composites to which the mesophase was added. With carbonization at 600°C, volatilization of small molecules from phenolic resin and oxidative PAN fiber felts contributed to the weight loss of all of the composites. The curves that plotted weight loss in various composites continuously rose as the carbonization temperature was increased to 1000°C. A substantial increase in weight loss of various composites was caused by the volatilization of small molecules from the phenolic resin and oxidative PAN fiber felts. Under the same carbonization conditions, the weight loss of the phenolic resin carbonized to 1000°C was approximately 40 wt % and that of the oxidative PAN fibers was about 50 wt %.[16] The weight losses of the R0, M10, and M30 composites were 37.3, 34.5, and 31.7 wt %, respectively. The weight loss in

the composite R0 was lower than total weight loss of the phenolic resin and oxidative PAN fibers, suggesting that the phenolic resin interacted with the oxidative PAN fibers. As the temperature was increased from 600 to 1000°C, the weight loss in various composites thus increased: not only were small molecules volatilized from the phenolic resin and PAN fiber felts, but also volatile gases such as H_2O, CO, and CO_2 were volatized by chemical reactions to form a strong interface between the phenolic resin and oxidative PAN fibers. The weight loss of all composites above 1500°C tended to change only moderately because most small molecules were released above this temperature. When the R0, M10, and M30 composites were graphitized at 2500°C, their weight losses were 41.5, 37.0, and 34.6 wt %, respectively. The weight loss of sample M30 was lower than that of sample R0 following carbonization and graphitization, which revealed that the small amount of volatiles released from the mesophase spheres were more stable than the phenolic resin during carbonization and graphitization.

Figure 2(b) demonstrates the linear shrinkage of the composites versus the heat-treatment temperature (HTT) increases. The amount of shrinkage depended on the type of polymer matrix used to fabricate the composites and the fiber–matrix interaction. For the initial carbonization at 600°C, the shrinkage of all of the composites was in the range 7.3–9.5%. This shrinkage was associated with condensation and crosslinking reactions of polymeric structures to form glassy carbon. Furthermore, heat treatment to 1000°C sharply accelerated the shrinkage of all composites to a range of 13.7–16.3%; the rearrangement of the carbon structure was the main cause. Above 1000°C, the shrinkage of all composites remained almost constant within the range 15–16.8% and was very slow due to the repacking and crosslinking of the glassy carbon structure. Heat treatment at 1800°C triggered the conversion of nongraphitic carbon into a graphitelike carbon structure and a reorientation of the graphite planes. Nitrogen contained in the functional groups on the surface of the oxidative PAN fibers was released, causing a small volume expansion. Therefore, a small decrease in the shrinkage of all of the composites was observed. Additionally, heat treatment at 2500°C caused a small increase in the shrinkage for all of the composites because of a more extensive reorientation of the graphitic plane. At 2500°C, the linear shrinkages were 17.4% for R0, 16.3% for M10, and 14.2% for M30.

Our experiments revealed how the addition of the mesophase changed the weight loss, shrinkage, and microstructure of the glasslike carbon. The addition of the mesophase MCMBs retarded the polymerization of the resin, reduced weight loss, and limited the shrinkage during heat treatment. A decrease in the carbonization weight loss and shrinkage as the mesophase MCMB was added was noted. The weight loss and shrinkage of composites M10 and M30 improved by approximately 20 and 18 wt %, respectively, over that of composite R0.

TABLE I
Variation in the Bulk Densities of the Composites

	Bulk density (g/cm^3)		
HTT (°C)	R0	M10	M30
600	1.48	1.44	1.34
1000	1.59	1.57	1.39
1300	1.52	1.57	1.60
1500	1.48	1.50	1.51
1800	1.37	1.40	1.53
2500	1.25	1.31	1.41

Density and open pores

Bulk density is the density of the composites, including voids and porosity. Table I shows the density versus HTT, as influenced by dimensional change due to shrinkage and weight loss from the evolution of volatile products during pyrolysis. After heat treatment at 600°C, the bulk density was 1.48 g/cm^3 for composite R0, 1.44 g/cm^3 for M10, and 1.34 g/cm^3 for M30. Disparity between the shrinkage of the mesophase and that of the phenolic resin caused the formation of pores and cracks around the mesophase spheres MCMBs, as shown in Figure 9(b). Pores and cracks in composites M10 and M30 caused their bulk densities to be less than that of composite R0. At 600–1000°C, the bulk density of all of the composites rose continuously, with shrinkage more rapid than weight loss. The maximum bulk density of R0 was 1.59 g/cm^3, that of M10 was 1.52 g/cm^3, and that of M30 was 1.43 g/cm^3. Above 1500°C, the bulk density of all of the composites dropped abruptly because of the formation of closed micropores in the phenolic resin matrix.[19] Heat treatment at 2500°C yielded a final bulk density of 1.25 g/cm^3 for R0, 1.31 g/cm^3 for M10, and 1.41 g/cm^3 for M30.

Figure 3(b) shows the changes in the real density of composites. In this study, an AccuPyc 1330 pycnometer was used to calculate the real density of the composites. For the AccuPyc 1330 pycnometer, pure helium gas was used to measure the volume of the composites. This gas could enter pores of 0.22 nm when helium gas was used to measure the volume of the composites, so the real density of composites was considered the density of the composites, only with voids. Initially, at 600°C, the real density of all of the composites was in the range 1.25–1.46 g/cm^3. Above 600°C, the polymeric structure of the resin was gradually transformed into the glassy carbon structure, and evolved gases passed easily through preexisting pores without further expansion. At this time, chemical densification dominated variation in density; the dominant factor during pyrolysis was the formation of

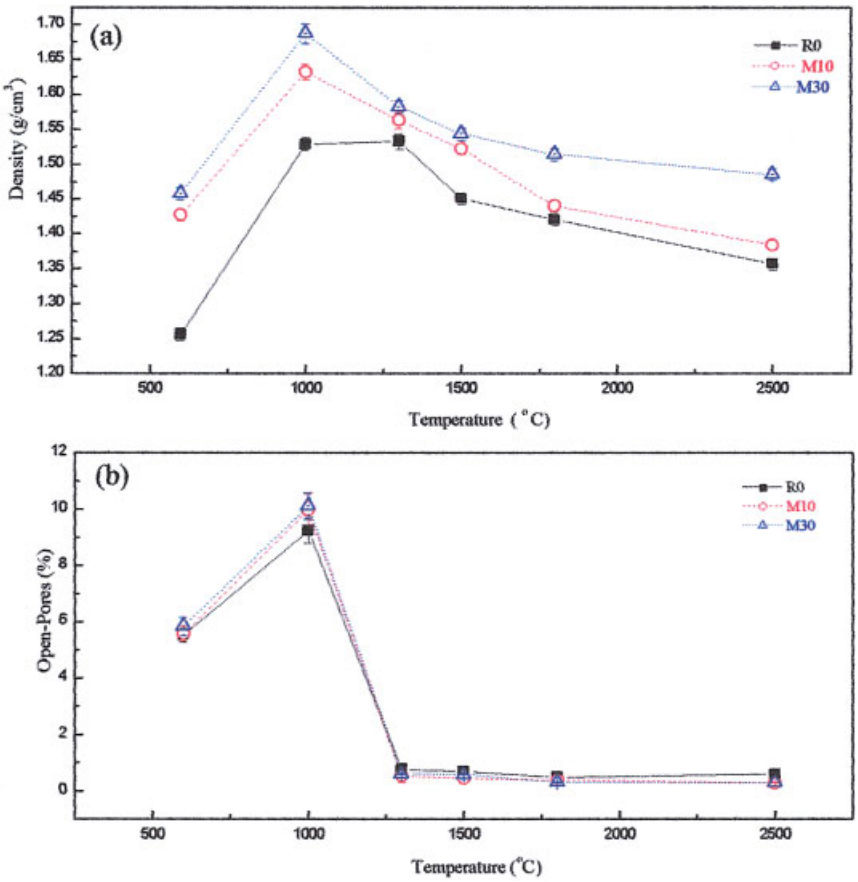

Figure 3 Change in the (a) real density and (b) friction volume of open pores in the composites at different HTTs.

new pores. The real density of composites M10 and M30 declined sharply between 1000 to 1800°C; the decrease for composite M10 was moderate, from 1.44 to 1.38 g/cm^3, and that for composite M30 was minor, from 1.51 to 1.49 g/cm^3. Composite R0 exhibited a smaller decrease from 100 to 1300°C but with a sharp drop above 1300°C. The bulk density also fell abruptly because of the formation of closed micropores in the phenolic resin matrix. At 2500°C, the final real densities were 1.36 g/cm^3 for R0, 1.39 g/cm^3 for M10, and 1.49 g/cm^3 for M30.

Figure 3(b) plots the variation in the fractional volume of the open porosity of the composites with HTT. Initially, at 600°C, the friction volume of the open pores was 5.5% for composite R0, 5.57% for M10, and 5.84% for M30. The friction volume of the open pores of the composites increased rapidly below 1000°C and maximized for all composites at 1000°C; the friction volumes of pores in the R0, M10, and M30 composites were 9.24, 9.98, and 10.11%, respectively. Differences in the shrinkage of the mesophase spheres MCMBs versus the phenolic resin matrix caused the formation of numerous pores and cracks that surrounded the mesophase spheres MCMBs, which explained why the friction volume of the pores in composites M10 and M30 exceeded that of composite R0. At 1000–1300°C, the heat increased the number of microcracks and promoted the formation of closed pores,[20,21] reducing the number of open pores and the density of all of the samples. Aromatization and crosslinking among heterocyclic rings, plus the lengthening and broadening of carbon-based planes, led to the repacking of the structure in the resin. These reactions led to the conversion of open pores to closed pores and reduced the density. At 2500°C, the friction volumes of open porosity of the R0, M10, and M30 composites were 0.59, 0.3, and 0.29%, respectively.

X-ray diffraction (XRD) and *Lc*

XRD is used extensively to obtain information about the structures of carbon materials. In the XRD patterns of carbon materials, peaks (002), (004), (004), (101), and (110) reveal the crystalline order in carbon.[22] Figure 4 displays the X-ray patterns for a composite following pyrolysis at various temperatures. Figure 4 indicates these patterns showed a broad peak at $2\theta \approx 22.4°$ for composite R0, one at $2\theta \approx 23.19$ for M10, and one at $2\theta \approx 25.36°$ for M30. For R0, a broad and weak peak at $2\theta \approx 22.4°$ was associated with the transformation of noncarbon materials in the phenolic resin into glass carbon. Composites M10 and M30 included two

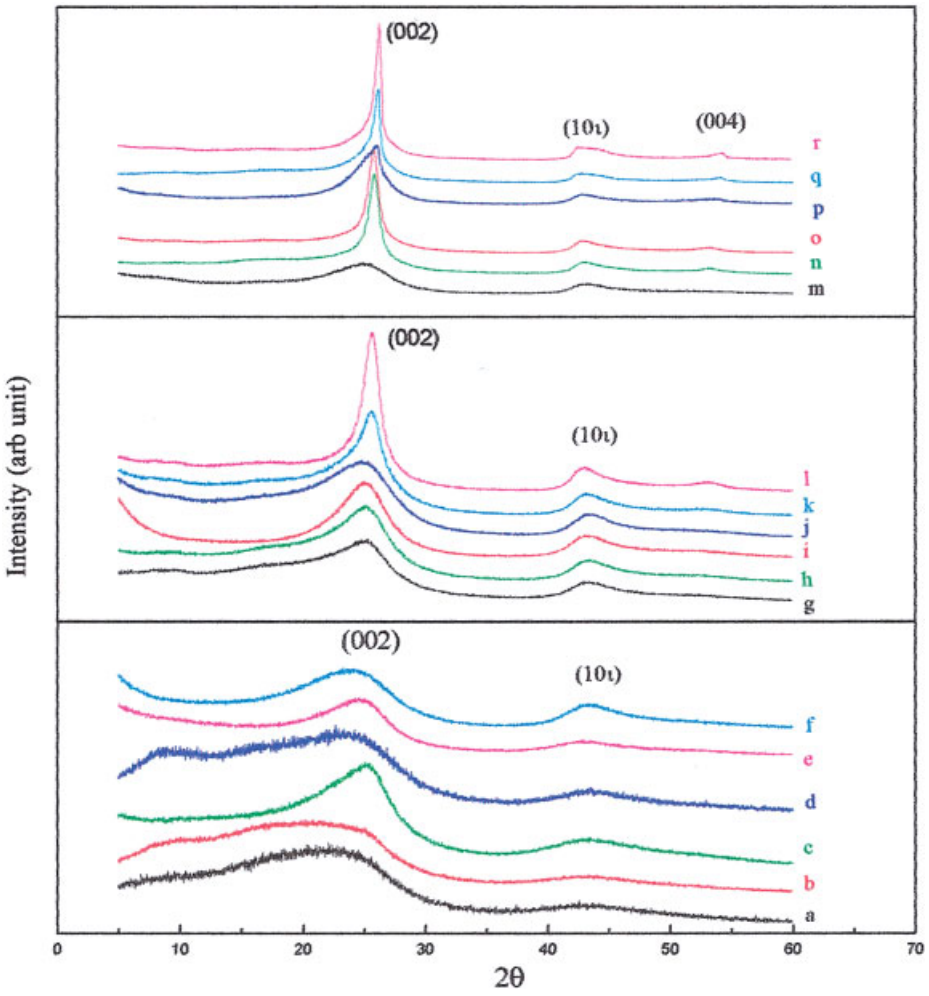

Figure 4 Changes in the XRD patterns of the composites at different HTTs: (a) R0 at 600°C, (b) M10 at 600°C, (c) M30 at 600°C, (d) R0 at 1000°C, (e) M10 at 1000°C, (f) M30 at 1000°C, (g) R0 at 1300°C, (h) M10 at 1300°C, (i) M30 at 1300°C, (j) R0 at 1500°C, (k) M10 at 1500°C, (l) M30 at 1500°C, (m) R0 at 1800°C, (n) M10 at 1800°C, (o) M30 at 1800°C, (p) R0 at 2500°C, (q) M10 at 2500°C, and (r) M30 at 2500°C.

peaks: one associated with the phenolic resin and the other associated with the mesophase spheres MCMBs. At 600–1500°C, the intensities of peaks corresponding to (002) and (10ι) *B* for carbon increased with HTT, and patterns revealed structure of sample R0 as amorphous. The addition of the mesophase spheres MCMBs caused the intensity of peaks of the (002) and (10ι) planes to rise faster with temperature. Heat treatment at 1800°C precipitated the conversion of nongraphite carbon in a graphitelike carbon structure. Unlike the patterns of composites M10 and M30, those of composite R0 were somewhat amorphous, in that the phenolic resin was hard carbon. Furthermore, continuously raising HTT to 2500°C caused the intensities of the peaks at (002) and (10ι) *B*s to become stronger and the half-width of the peak of the (002) basal plane of the carbon to decline, as shown in Figure 4, because the graphitic planes' reorientation grew more extensive. Table II lists the L_C values of the (002) plane and the interlayer spacing (d_{002}) of the composites after pyrolysis at various temperatures. For all of the composites, the interlayer spacing clearly decreased, whereas L_C increased very slowly with the rise in HTT. Notably, the addition of the mesophase spheres effectively raised L_C at 2500°C, yielding a L_C of 3.1 nm for composite R0, 10.99 nm for composite M10, and of 18.20 nm for composite M30.

Raman spectra analysis

The Raman spectrum is a useful tool for obtaining information on the microstructure of carbonaceous material.[23] In this study, a Raman spectrum associated with $\lambda = 632.8$ nm obtained with a 25-W He–Ne laser was considered to typify the microstructure. Thus, eqs. (2) and (3) specify R and L_a. Figure 5 shows the changes in the fitted Raman spectra of the composites during pyrolysis. Above 1000°C, the Raman spectra revealed two strong wide bands near 1580 and 1360 cm^{-1}. A peak near 1580 cm^{-1} was associated with the

TABLE II
XRD Results of the R0, M10, and M30 Composites Treated at Various Temperatures

	Carbonization and graphitization temperature (°C)					
	600	1000	1300	1500	1800	2500
Sample R0						
2θ (°)	22.438	24.403	25.353	25.362	25.334	25.381
d (nm)	0.397	0.362	0.358	0.354	0.352	0.350
L_C (nm)	0.861	1.363	1.438	1.674	2.259	3.104
Sample M10						
2θ (°)	23.192	24.954	25.138	25.354	25.758	26.133
d (nm)	0.373	0.359	0.354	0.348	0.353	0.341
L_C (nm)	0.878	1.398	2.214	2.633	6.787	10.992
Sample M30						
2θ (°)	25.361	25.456	25.153	25.956	25.964	26.151
d (nm)	0.364	0.354	0.348	0.342	0.337	0.341
L_C (nm)	0.959	1.543	2.353	3.073	9.129	18.200

graphitic structure (D band), and any peaks near 1360 cm^{-1} were associated with a disordered structure (G band) in carbon. An increase in the order in carbonaceous materials is well known to be reflected by an increased frequency of the G mode and/or a decreased frequency of the D mode. Figure 5 shows the G-mode peaks elevating and the D-mode peaks declining as the temperature increased. In the case of composite M30, the intensity of the G-mode peak exceeded that of the D-mode peak following pyrolysis at 1800°C, whereas that of the G-mode peak exceeded that of the D-mode peak for composites R0 and M10 following pyrolysis at 2500°C. Table III lists the L_a and R values of the composites following pyrolysis at various temperatures. For composites R0 and M10, the initial L_a value range was 0.75–1.39 nm. Furthermore, the rise in the L_a value was smooth between 600 and 1500°C. Heat treatment at 1800°C abruptly increased L_a for composites R0 and M10 because the reorientation of the graphitic planes in carbon began at 2500°C; the L_a values of composites R0 and M10 were 3.86 and 4.78 nm, with the graphitic plane in carbon extensively reoriented. For composite M30, L_a rose slightly (1.68 to 1.8 nm) at 600–1000°C. Moreover, L_a remained almost the same between 1000 to 1500°C. The large increase in L_a in composite M30 was from 1.8 to 5.0 nm at HTTs from 1500 to 2500°C. The changes in the Raman spectra of the R0, M10, and M30 composites demonstrated the nongraphitizable feature of carbon for a phenolic resin and the graphitizable feature of carbon for mesophase. Notably, the addition of the mesophase MCMBs effectively increased L_a and the crystallinity of the composites.

Polarized optical microscopy

Polarized light is often used to observe interference color generated by the orientation of graphitic lamellae at the surface.[24,25] Figure 6 traces the polarized light optical micrographs of these C/C composites at various temperatures, along with a cross-polarized light micrograph of composites heat-treated at various temperatures. For composite R0, bonding between the fibers and the matrix was strong because many functional groups were present on the surface of the oxidative PAN fiber, as depicted in Figure 6(a–c). The core of fibers was represented by light blue and bright blue colors at 600, 1500, and 2500°C, indicating the fibers had an anisotropic texture and that heat treatment enhanced the preferred orientation of the carbon layer in the fibers. The matrix had an isotropic texture, as indicated by the purple color in the matrix. The matrix derived from the phenolic resin was nongraphitizable carbon with a glasslike isotropic texture. After graphitization at 2500°C, the preferential orientation of the matrix was parallel to the fiber axis around the fibers, as revealed by the micrographs in Figure 6(c). In the area around the fibers, the matrix was graphitized and exhibited a preferred orientation of the carbon layers with an isotropic texture because stress orientation arose from strong bonding between the fiber and the matrix, which formed a region oriented parallel to the fiber surface at the interface of the fibers. In the case of composites M10 and M30, as in Figures 6(d–i), the mesophase spheres clearly exhibited light blue and bright blue colors at 600, 1500, and 2500°C, respectively, which revealed that the mesophase spheres MCMBs and fibers had an anisotropic texture. On the other hand, at 2500°C, the small areas around microcracks surrounding mesophase in composites M10 and M30 showed light blue colors. It also indicated an anisotropic texture; thermal stress caused by differing thermal shrinkage rates of the phenolic resin and mesophase engendered an anisotropic texture, thus helping to improve the flexural strength and moduli of composites M10 and M30 above 1800°C. The micrographs revealed that the microcracks surrounding the mesophase spheres MCMBs were formed by the difference between the shrinkage rates of the phenolic resin and the mesophase MCMBs.

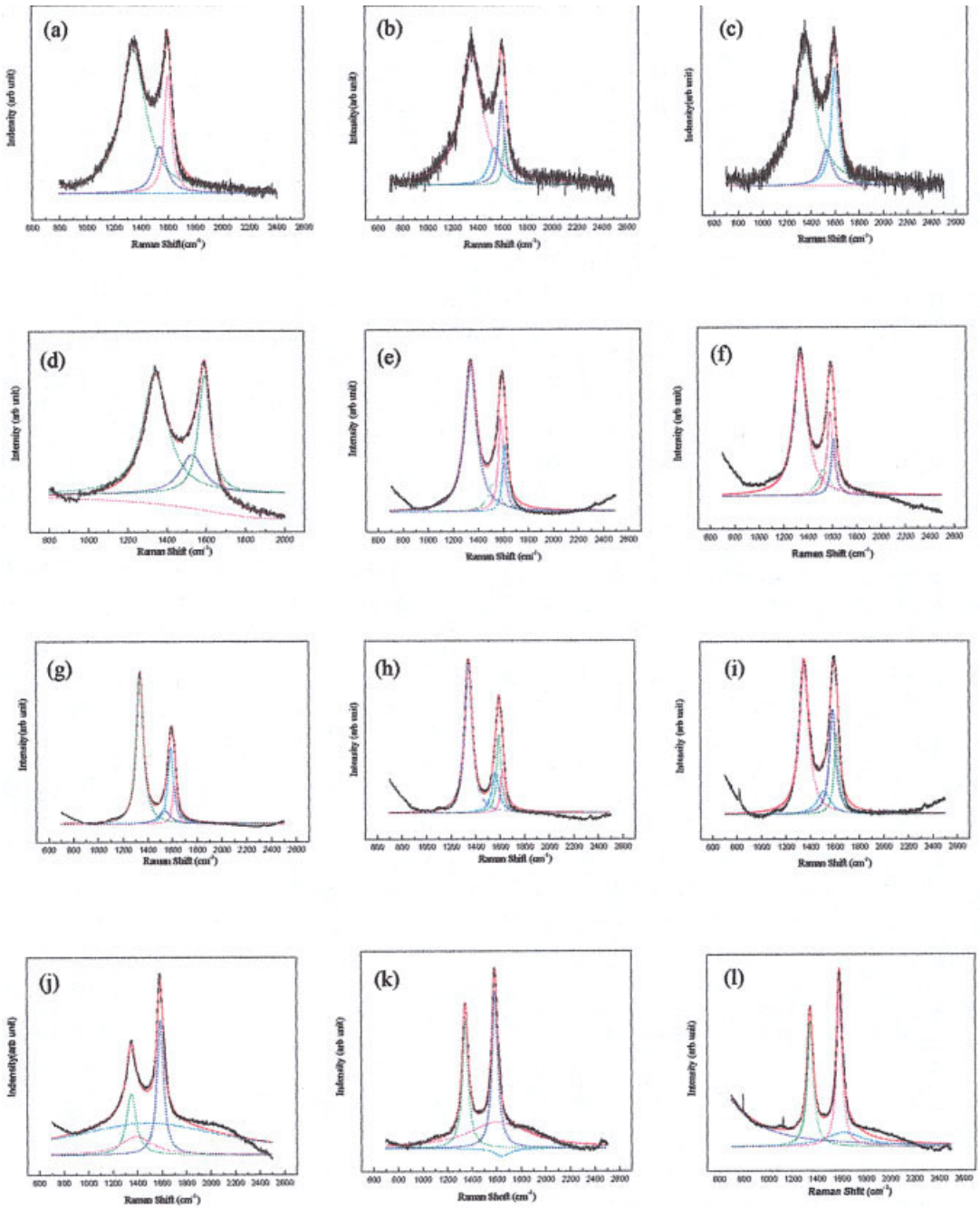

Figure 5 Changes in the fitted Raman spectra of composites during pyrolysis: (a) R0 at 1000°C, (b) M10 at 1000°C, (c) M30 at 1000°C, (d) R0 at 1500°C, (e) M10 at 1500°C, (f) M30 at 1500°C, (g) R0 at 1800°C, (h) M10 at 1800°C, (i) M30 at 1800°C, (j) R0 at 2500°C, (k) M10 at 2500°C, and (l) M30 at 2500°C.

Mechanical properties

Figure 7(a) shows the model used to measure the mechanical properties. Figure 8 plots the variations in the flexural strengths and moduli of the R0, M10, and M30 composites versus temperature at 600–2500°C. Figure 8 reveals how the initial flexural strengths and moduli of all of the composites at 600°C were low because of the condensation of the polymer structures in the resin[26] and crosslinks in the oxidative PAN fiber felts.[27] Additionally, abrupt increases in the flexural strength for all composites were observed at 600–1000°C. In this phase, carbon basal planes formed from the ladder polymer, increasing the preferred orientation, density, and modulus.[28] However, glass carbon structures were transformed into isotropic carbon structures in the matrix resin. These reactions increased the flexural strength and modulus of the composites, such that they led to lower flexural strength and moduli values for the M10 and M30 composites compared to those of R0. From 1000 to

TABLE III
Raman Spectra Results of the R0, M10, and M30 Composites Treated at Various Temperatures

Temperature (°C)	Composite type					
	R0		M10		M30	
	I_D/I_G	L_a (nm)	I_D/I_G	L_a (nm)	I_D/I_G	L_a (nm)
600	5.87	0.75	3.16	1.39	2.62	1.68
1000	3.86	1.14	3.41	1.29	2.44	1.8
1300	3.76	1.17	3.45	1.27	2.46	1.79
1500	3.66	1.20	3.54	1.36	2.45	1.80
1800	2.07	2.13	1.78	2.48	1.46	2.74
2500	1.14	3.86	0.92	4.78	0.88	5.00

1500°C, the flexural strengths and moduli of all of the composites decreased quickly by virtue of an increase in microcracks and the formation of closed pores. Above 1800°C, the flexural strength of all of the composites increased slightly because the conversion of nongraphite carbon in a graphitelike carbon structure begins. At 2500°C, the flexural strengths were 15.4 MPa for R0, 18.4 MPa for M10, and 22.4 MPa for M30. A continuous decline in the flexural moduli of composite R0 was observed above 1800°C, whereas the flexural moduli of composites M10 and M30 increased slightly. At 2500°C, the flexural moduli were 1.65 GPa for R0, 1.9 GPa for M10, and 2.4 GPa for M30.

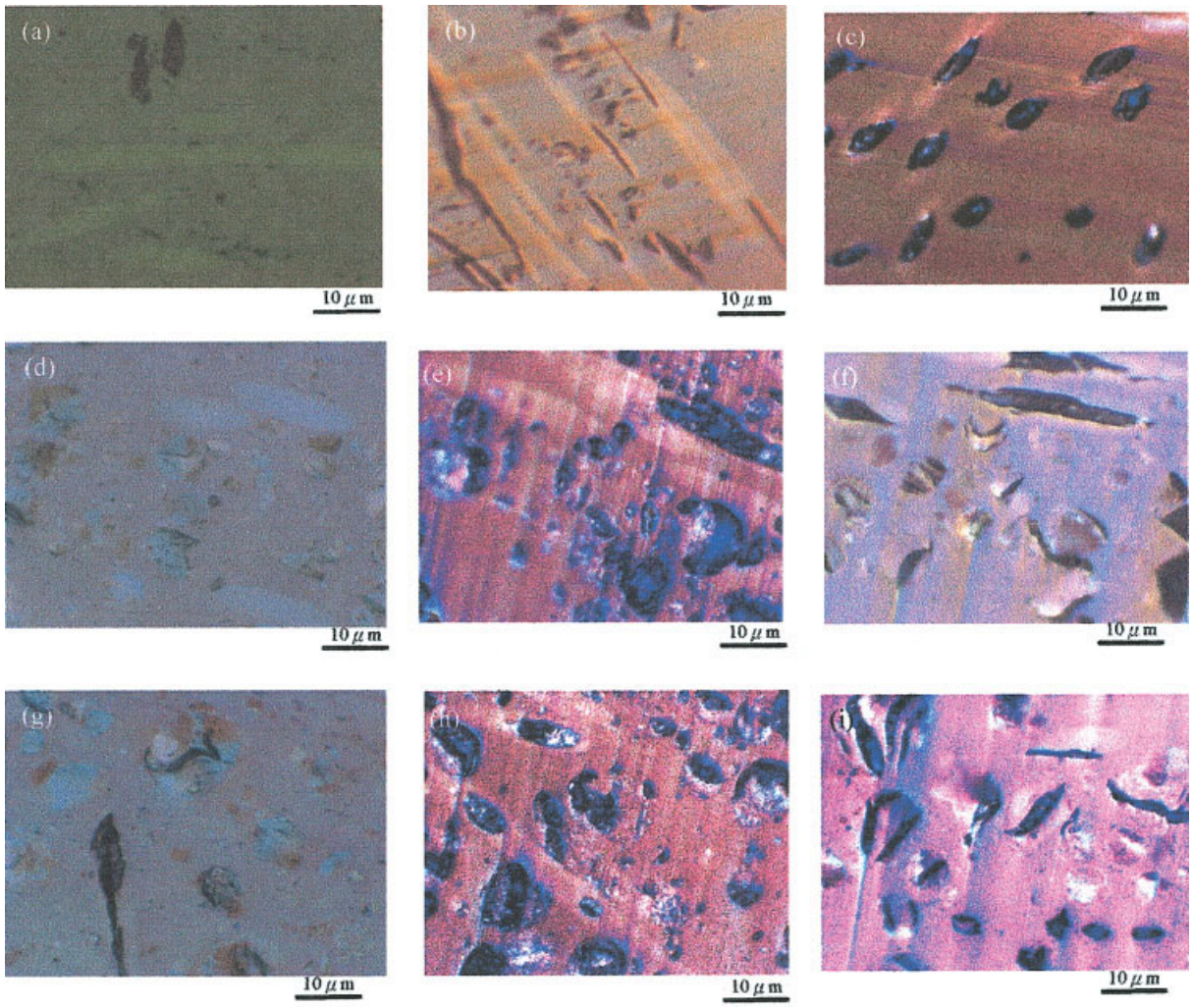

Figure 6 Polarized light optical micrographs of C/C composites at different HTTs: (a) R0 at 600°C, (b) R0 at 1500°C, (c) R0 at 2500°C, (d) M10 at 600°C, (e) M10 at 1500°C, (f) M10 at 2500°C, (g) M30 at 600°C, (h) M30 at 1500°C, and (i) M30 at 2500°C.

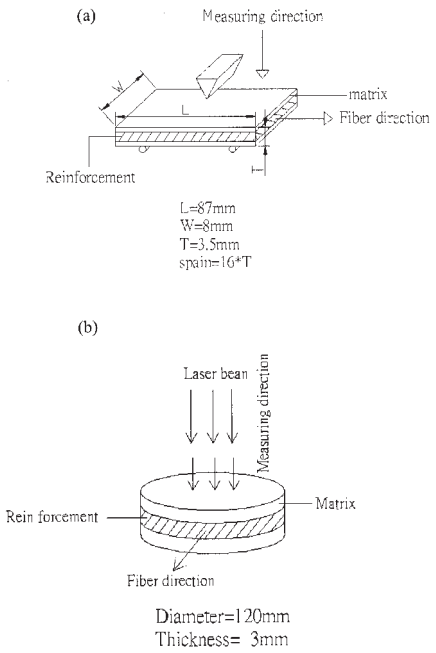

Figure 7 Illustrations of the (a) three-point bending tests and (b) thermal conductivity measurement for the C/C composites.

In this study, the flexural strength and moduli of composites M10 and M30 were lower than those of R0 below 1800°C. However, the flexural strengths and moduli of composites M10 and M30 exceeded those of R0 above 1800°C. Below 1800°C, pores and cracks that surrounded the mesophase spheres MCMBs [Figs. 2(b) and 9(b)] in composites M10 and M30 became centers of stress concentration and propagation, which made the flexural strengths and moduli of these composites lower than those of R0.

Above 1800°C, these small areas surrounding the mesophase spheres MCMBs and microcracks in the phenolic matrices showed an anisotropic texture [Figs. 6(h,i)]. Such an anisotropic texture (graphitizable carbon) emanated from both interface bonding and interface stress between the mesophase spheres and phenolic resin. The interface stress was caused by different shrinkage rates between the mesophase spheres MCMBs and phenolic resin during graphitization. The mesophase spheres MCMBs were extracted from coal tar in air at 400–600°C, so the mesophase spheres MCMBs also had some functional groups. These functional groups in both the phenolic resin and the mesophase took chemical reactions to from strong interface bonding during the curing process and interface bonding between the oxidative fibers and resin. Ko et al.[29] reported that interface bonding between oxidative fibers and a phenolic resin caused a small anisotropy texture around fibers after graphitization. Ko et al. also described small anisotropy textures around fibers enhancing flexural strength and moduli. In this

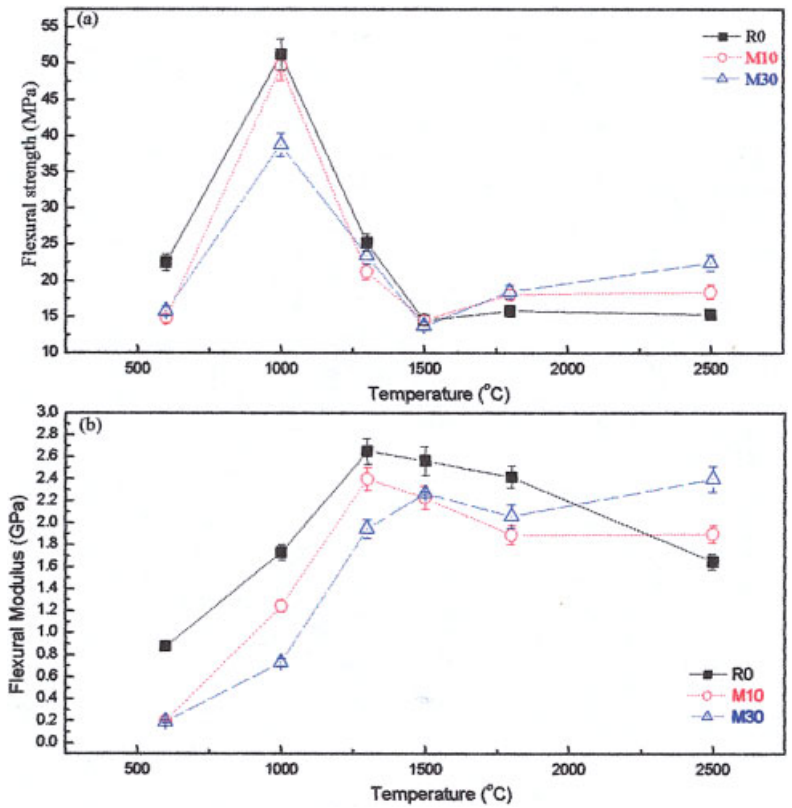

Figure 8 Changes in the (a) flexural strength and (b) flexural modulus of the R0, M10, and M30 composites with HTT in the range 600–2500°C.

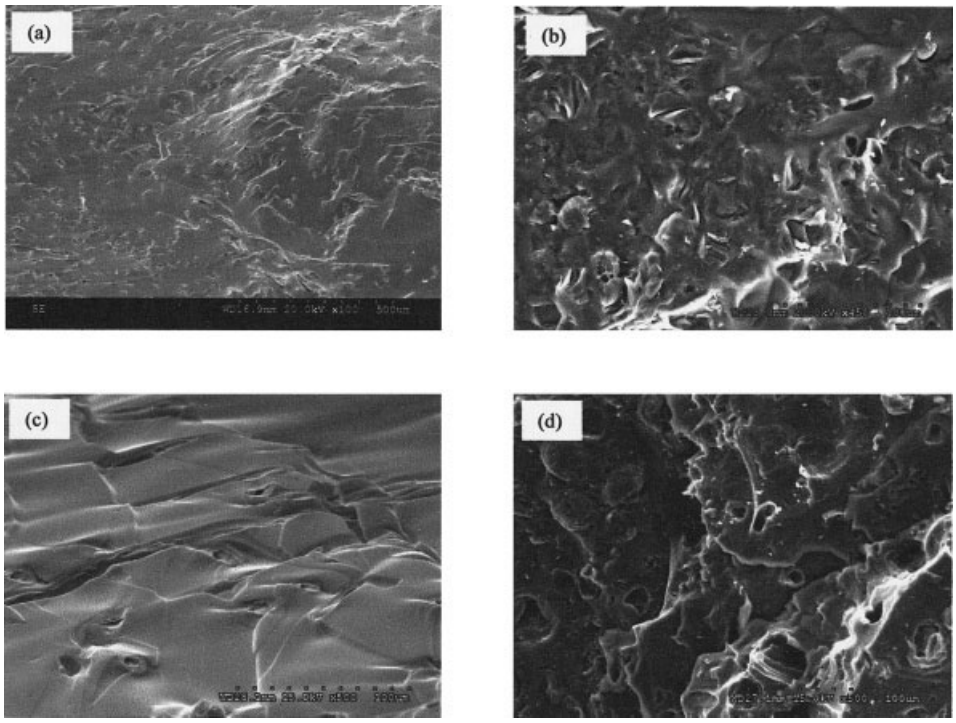

Figure 9 Morphologies of the fracture planes of the composites after the three-point bending test: (a,b) R0 after pyrolysis at 1000°C and (c,d) R0 after pyrolysis at 2500°C.

study, these small anisotropic textures surrounding the mesophase spheres MCMBs and microcracks were regard as a factor in the increase of the flexural moduli of composites M10 and M30, compared with composite R0. For the flexural strength, these interface stresses between the mesophase spheres and the resin in composites M10 and M30 above 1800°C also played an important role. Interface stress blocked or changed the direction of microcrack propagation and, thereby, caused an increase in the flexural strength in composites M10 and M30, as compared with composite R0.

Electrical resistance and thermal conductivity

Electrical resistance depends on the extent of crystallinity and the orientation of the layer planes in carbon. It declines in carbon when crystallinity increases. Accordingly, the addition of the mesophase spheres MCMBs was expected to reduce the electrical resistance of the C/C composites derived from oxidative PAN fiber felts and the phenolic resin because the mesophase MCMB exhibited good crystallinity. Figure 10 displays the electrical resistance of the composites at various temperatures. At 1000°C, the electrical resistances were 1.8×10^{-2} Ω cm for R0, 6.7×10^{-3} Ω cm for M10, and 5.97×10^{-3} Ω cm for M30. Likewise, the electrical resistance in all of the composites fell quickly between 1000 and 1300°C. Above 1300°C, all of the composites showed a moderate decline. At 2500°C, the electrical resistances were 4.26×10^{-3} Ω cm for R0, 3.7×10^{-3} Ω cm for M10, and 2.45×10^{-3} Ω cm for M30. The electrical resistance of any composite fluctuated with the HTT and crystallinity of the composites.

Thermal conductivity is a critical feature of C/C composites, especially those used in brake disks on aircraft. The thermal conductivity of carbon is directly proportional to mean path of a phonon.[30] Phonon scattering also depends on the extent of crystallinity and the orientation of layer planes. Figure 7(b) shows the model used to measure thermal conductivity: the laser beam and measuring direction are transverse to the direction of the fibers. Table IV presents the thermal conductivity results in the transverse direction of the fibers. Clearly, the thermal conductivity increased with HTT and the amount of mesophase spheres MCMBs added. At 2500°C, the thermal conductivities were 6.7 W/mk for R0, 7.5 W/mk for M10, and 8.8 W/mk for M30. In this study, the measured electrical resistance and thermal conductivity provided evidence that these properties depended strongly on the crystallinity of the C/C composites and that mesophase spheres MCMBs boosted the electrical resistance and thermal conductivity by promoting the crystallinity of the C/C composites derived from oxidative PAN fiber felts and the phenolic resin.

CONCLUSIONS

The influence of adding mesophase MCMBs to the microstructure, physical characteristics, electrical resistivity, and thermal conductivity of C/C composites

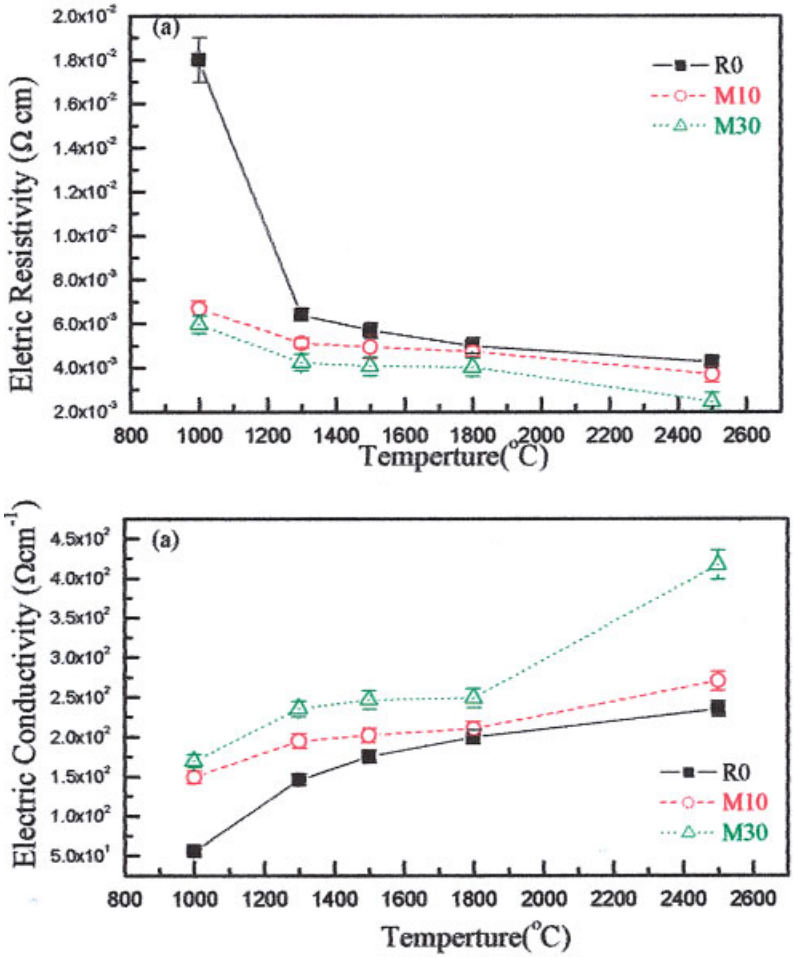

Figure 10 Changes in the (a) electrical resistivity and (b) electrical conductivity of the composites at different HTTs.

prepared by pyrolyzing oxidative PAN fiber felt/phenolic resin were gauged via heat treatment at 600–2500°C. XRD (L_C), Raman spectroscopy (L_a), and polarized light optical microscopy established differences between the microstructures of the resin and mesophase MCMB during cographitization. They revealed that mesophase and oxidative PAN fibers exhibited anisotropic textures, whereas the phenolic matrix had an isotropic texture following graphitization. This trait showed how the phenolic resin and mesophase were nongraphitizable and graphitizable carbon, respectively. The added mesophase thus augmented the electrical resistance and thermal conductivity of the C/C composites prepared from oxidative PAN fiber felt and the phenolic resin. Although the flexural strength and flexural moduli of the composites with mesophase MCMB added were lower than those without mesophase MCMB below 1500°C, the flexural strengths and flexural moduli of composites with mesophase exceeded those without mesophase MCMB above 1800°C. This may have been associated with the strengthening of the preferred orientation of the carbon layer plane with mesophase MCMB added to composites. This study's composites with 30 wt % mesophase showed improvement in thermal and electrical conductivity of 31.3 and 43.7%, respectively.

TABLE IV
Thermal Conductivity for the R0, M10, and M30 Composites After Heat Treatment at 1000 and 2500°C

Temperature (°C)	Thermal conductivity (W/mk)		
	R0	M10	M30
1000	1.55	1.57	1.78
2500	6.7	7.5	8.8

Measurement was normal to the direction of the carbon fiber.

References

1. Hüttener, W. Carbon Fibers Filament and Composites; Kluwer Academic: Boston, 1990; p 275.
2. Manocha, L. M. Sadhana Acad Proc Eng Sci 2003, 28, 349.
3. Savage, G. In Carbon–Carbon Composites; Chapman & Hall: London, 1993; Chapter 9.
4. Manocha, L. M.; Bhatt, H.; Manocha, S. M. Carbon 1996, 34, 841.
5. Ko, T. H. In Proceedings of the International Conference on Carbon, Essen, 1992; p 753.

6. Baxter, R. I, Rawlings, R. D.; Iwashita, N.; Sawada, Y. Carbon 2000, 38, 441.
7. Luo, R. Y.; Huai, X. L.; Qu, J. W.; Ding, H. Y.; Xu, S. H. Carbon 2003, 41, 2693.
8. White, J. L.; Sheaffer, P. M. Carbon 1989, 27, 697.
9. Mochida, I. Materially Speaking 1991, 7, 345.
10. Hu, H. L.; Ko, T. H.; Kuo, W. S. Polym Compos, to appear.
11. Cullity, B. D. Element of X-Ray Diffraction; Wesley: New York, 1978; p 99.
12. Tuinstra, F.; Koening, J. L., J Chem Phys 1997, 306, 17.
13. Watt, W. D.; Johnson, J.; Parker, E. In Proceedings of the International Conference on Carbon Fibers; Plastics Institute: London, 1974; p 3.
14. Fitzer, E.; Mueller, W.; Shaffer,; Walk, P. L.; Radovi, L. R. In Chemistry and Physics of Carbon; Marcel Dekker: New York, 1971; Vol. 7, p 7.
15. Kimberly, A.; Trick, E.; Tony, E. Carbon 1995, 33, 1509.
16. Ko, T. H.; Jaw, J. J.; Chen, Y. C. Polym Compos 1995, 16, 522.
17. Brook, J. D.; Taylor, G. H. Carbon 1965, 3, 185.
18. Lu, Y.; Ling, L.; Wu, D.; Liu, L.; Zhang, B. J Mater Sci 1999, 34, 4043.
19. Fizter, E. Carbon 1987, 25, 163.
20. Mehrotra, B. N.; Bragg, R. H.; Rao, A. S. J. Mater Sci 1983, 18, 2671.
21. Kipling, J. J.; Sherwood, J. N.; Shorter, P. V.; Thompson, N. R. Carbon 1964, 1, 321.
22. Pierson, H. O. Carbon, Handbook of Graphite, Diamond and Fullerenes; Noys: NJ, 1993; p 56.
23. Ferrari, A. C. Diamond Relat Mater 2002, 11, 1053.
24. Eswards, I. A. S.; Marsh, H. In Introduction to Carbon Science; Butterworths: London, 1989; p 19.
25. Cornford, C. R.; Forrest, A. B.; Kelly, T.; Marsh, H.; Walk, P. L.; Radovi, L. R. In Chemistry and Physics of Carbon; Marcel Dekker: New York, 1984; Vol. 19, p 211.
26. Hishiyama, Y. M.; Inagaki, K. S.; Yamada, S. Carbon 1974, 12, 249.
27. Donnet, J. B.; Wang, T. K.; Peng, J. C. Carbon Fibers; Marcel Dekker: New York; 1998; p 26.
28. Watt, W.; Johnson, W. Nature 1975, 257, 210.
29. Ko, T. K.; Kuo, W. S.; Chang, Y. H. Compos A 2003, 34, 393.
30. Bokros, J. C.; Walk, P. L.; Radovi, L. R. In Chemistry and Physics of Carbon; Marcel Dekker: New York, 1966; Vol. 5, p 1.